Sparse Scene Recovery for High-Resolution Automobile FMCW SAR via Scaled Compressed Sensing

Dae-Hwan Jung, Hyun-Seong Kang, Chul-Ki Kim, Junhyeong Park, *Graduate Student Member, IEEE*, and Seong-Ook Park, *Senior Member, IEEE*

***Abstract*— This paper introduces a sparse scene reconstruction algorithm for automobile frequency-modulated continuous-wave synthetic aperture radar (FMCW SAR) through scaled compressed sensing (CS). An FMCW radar leads to low manufacturing cost, compact realization, and low transmission power. An automobile SAR is more economical and easier to implement than typical SAR platforms (e.g., satellites and aircraft). We apply CS to randomly subsampled raw data of automobile FMCW SAR for sparse reconstruction. We exploit the fact that the velocity of an automobile is significantly lower than that of the SAR platforms, which leads to a vastly narrow bandwidth of an azimuth-matched filter in the azimuth compression of the range-Doppler algorithm (RDA). Low-frequency azimuth data have a fundamental effect on azimuth compression. We propose a new reconstruction scheme, scaled CS, which specializes in low-frequency information recovery for automobile SAR. The scheme is based on basis pursuit denoising (BPDN). A Ku-band FMCW SAR system is developed to verify the performance of the proposed algorithm. We mount our system on an automobile and collect FMCW SAR raw data in the stripmap mode with a van maintained a constant speed on a highway. The proposed reconstruction algorithm shows improved recovery performance for automobile FMCW SAR, which is validated by processing a high-resolution real SAR image.**

***Index Terms*— Automobile synthetic aperture radar (SAR), compressed sensing (CS), frequency-modulated continuous-wave (FMCW) radar, SAR, sparse reconstruction.**

I. Introduction

SYNTHETIC aperture radar (SAR) has been gaining popularity as it provides defined SAR images for surveillance in various research areas. The conventional SAR hardware system mounted on an aerospace platform is mostly a type of pulse radar that requires high peak transmission power. This leads to difficulties in generating high-power transmission pulse and the cost is high. Another type of radar, namely, frequency-modulated continuous-wave (FMCW) radar, has attracted attention as it leads to low manufacturing cost, small size, and low constant transmission power, which overcome the disadvantages of pulse radar systems [1]. In addition, advances in signal generation hardware [e.g., direct digital synthesizer (DDS) and high-speed digital-to-analog converter], which have ameliorated linear frequency modulation (LFM) with a wide sweeping bandwidth, have led to the emergence of a high-resolution FMCW radar system [2]–[4]. FMCW SAR was first demonstrated in 2007 [5] with a new signal processing algorithm only for FMCW SAR. Since then, there has been a special interest in FMCW SAR systems [6]–[9].

To guarantee a high-resolution SAR image, a high sampling rate is mandatory according to the traditional Nyquist sampling theorem. However, this requires an enormous amount of data, long computational time, and considerable cost. Recently, as an attractive alternative, compressed sensing (CS) has been proved to be applicable to SAR signal processing. CS can produce complete recovery of the original signal with fewer measurements than the Nyquist sampling rate. He *et al*. [10] combined CS with a multi-dictionary for SAR image reconstruction. In [11], a segmented reconstruction strategy for CS SAR imaging was introduced so that the reconstruction time could be significantly decreased. Unlike other authors, who did not consider range cell migration compensation (RCMC) in their studies, Bu *et al*. [12] presented the CS SAR imaging algorithm by considering RCMC as an intermediate step of its scheme. However, all aforementioned schemes are suitable for pulsed SAR. Therefore, the applicability of CS has been explored for FMCW radar systems [13]. Becquaert *et al*. [13] proposed CS SAR imaging, which can be applied to the randomly subsampled FMCW signal in the range and azimuth directions. Nevertheless, it is limited because sparse scenes containing only a few scatterers are used for them to be sparse and compressible in a transform domain. In contrast, FMCW SAR raw data acquired from outdoor experiments include many scatterers and are not sparse and compressible in the frequency domain; this is insufficient to satisfy the essential conditions of CS.

This paper proposes a new sparse scene recovery framework, i.e., scaled CS, for automobile FMCW SAR system. We analyze the limitation of CS reconstruction in both range

Manuscript received February 26, 2019; revised July 11, 2019; accepted July 24, 2019. Date of publication August 19, 2019; date of current version November 25, 2019. This work was supported by Institute of Information & communications Technology Planning & Evaluation (IITP) grant funded by the Korea government (MSIT) (No.2018-0-01658, Key Technologies Development for Next Generation Satellites). *(Corresponding author: Dae-Hwan Jung.)*

The authors are with the School of Electrical Engineering, Korea Advanced Institute of Science and Technology, Daejeon 34141, South Korea (e-mail: daeman88@kaist.ac.kr; kanghs77@kaist.ac.kr; chulki@kaist.ac.kr; bdsfh0820@kaist.ac.kr; soparky@kaist.ac.kr).

Color versions of one or more of the figures in this article are available online at http://ieeexplore.ieee.org.

Digital Object Identifier 10.1109/TGRS.2019.2931626

and azimuth for FMCW SAR. The azimuth and range data are neither sparse nor compressible in the frequency domain due to the presence of many scatterers. Thus, it is impossible to perfectly reconstruct FMCW SAR raw data. Nevertheless, we apply CS to the raw data for sparse reconstruction. We also show that the capability of CS to recover a sparse scene can be significantly improved. We experiment with an automobile as a radar platform to obtain SAR raw data. This so-called automobile SAR experiment offers benefits of easy modification and low cost compared to the case in which the system is equipped on conventional SAR platforms (e.g., satellite and airplane) [14]–[16]. It is also noted that the speed of an automobile is considerably slower than that of other SAR platforms. When the radar platform is an automobile, an azimuth-matched filter applied to the azimuth compression stage of the range-Doppler algorithm (RDA) not only has a narrow bandwidth but also operates as a low-pass filter. The low-frequency information of azimuth data spread out in the Doppler frequency domain has a dominant effect on azimuth focusing for single-look processing. In other words, we only need low-frequency data within the bandwidth of the filter to pass through for azimuth compression. Despite not being sparse or compressible, we can assume that the data required for azimuth compression are sparse and compressible in the frequency domain. This means that we can exploit CS to reconstruct SAR images from the subsampled raw signal. Significantly, the conventional CS focuses on the recovery of all frequency data instead of the low-frequency data. To that end, we here propose a new reconstruction method, called scaled CS, which is a modification of basis pursuit denoising (BPDN) and improves the recovery performance of low-frequency signals.

The remainder of this paper is organized as follows. Section II introduces an automobile FMCW SAR signal model. Section III provides a new reconstruction scheme for automobile FMCW SAR through scaled CS. Section IV-A describes the developed FMCW SAR system using DDS, which can yield high-resolution images. Section IV-B explains an automobile FMCW SAR experiment conducted on a highway. Section V presents the experimental results reconstructed by the proposed algorithm with the analysis. Finally, conclusions for this paper are drawn in Section VI.

II. Automobile FMCW SAR Signal Model

In this section, we introduce an automobile FMCW SAR signal model to emphasize the characteristic of the automobile platform. The signal transmitted from an FMCW radar can be described as follows [17]:

$$s_{\mathrm{TX}}(t) = \exp\left\{ j2\pi \left(f_c t + \frac{1}{2}\frac{B_{\mathrm{swp}}}{T_{\mathrm{swp}}} t^2 \right) \right\} \tag{1}$$

where f_c is the carrier frequency, t is the time variable within the pulse repetition interval (PRI), B_{swp} is the LFM sweep bandwidth of the transmitted baseband signal, and T_{swp} is PRI. B_{swp} and T_{swp} are constants because we assume that LFM is applied to generate a baseband signal. We also assume that the system uses an ideal linear chirp modulation, which means that an additional calibration technique for residual-video-phase removal is unnecessary. After reflecting off K stationary targets, the received radar signal is given as follows [18]:

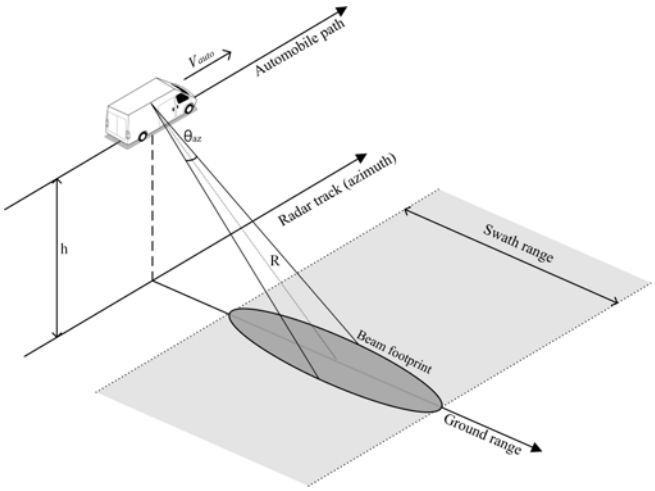

Fig. 1. Automobile FMCW SAR geometry in the zero-squint case.

$$s_{\mathrm{RX}}(t) = \sum_{k=1}^{K} \exp\left\{ j2\pi \left(f_c(t-\tau_k) + \frac{1}{2}\frac{B_{\mathrm{swp}}}{T_{\mathrm{swp}}}(t-\tau_k)^2 \right) \right\} \tag{2}$$

where τ_k is the time delay generated by the kth target and is expressed as follows:

$$\tau_k = \frac{2R_k}{c} \tag{3}$$

where R_k is the kth target range and c is the speed of light. After mixing with the transmitted and received signals by a mixer, the obtained intermediate frequency is expressed as follows:

$$s_{\mathrm{IF}}(t) = \sum_{k=1}^{K} \exp\left\{ j2\pi \left(-f_c\tau_k - \frac{B_{\mathrm{swp}}}{T_{\mathrm{swp}}}\tau_k t + \frac{1}{2}\frac{B_{\mathrm{swp}}}{T_{\mathrm{swp}}}\tau_k^2 \right) \right\}. \tag{4}$$

The target range information can be extracted from the second phase term of (4) called beat frequency, which is a sinusoidal signal proportional to the time delay. We extract the frequency information using a Fourier transform. Using (3) and (4), the target range can be derived as follows:

$$R_k = \frac{\mathrm{cT_{swp}}\, f_{\mathrm{beat},k}}{2B_{\mathrm{swp}}}. \tag{5}$$

In terms of digital data acquisition, the maximum target range is determined by the highest beat frequency stored, which is limited by the sampling rate in the data acquisition process. Hence, the sampling rate needs to be increased to obtain a wide swath range. In addition, as the range resolution is inversely proportional to the sweep bandwidth, a wide sweep bandwidth is required to obtain a high range resolution for FMCW SAR images. In contrast, widening the bandwidth causes a decrease in the pulse repetition frequency (PRF). The fact that the Doppler bandwidth is larger than the PRF results in azimuth ambiguity because of aliasing caused by a lack of sampling rate.

An automobile FMCW SAR geometry in the zero-squint case is shown in Fig. 1. As an automobile platform moves

along its path with its velocity V_{auto}, the strength of the received signal varies with azimuth time η due to an azimuth beam pattern. Then, the demodulated received signal after the range compression of RDA can be expressed by [19]

$$S_{\text{rc}}(f_\tau, \eta) \approx \sum_{k=1}^{K} A_{0,k}\, W_r[f_\tau - f_{\text{beat},k}]\omega_a(\eta - \eta_c) \times \exp\left\{-j\frac{4\pi f_c R_0}{c}\right\} \exp\{-j\pi K_a \eta^2\} \tag{6}$$

where $A_{0,k}$ is the magnitude of the kth target, which indicates the backscatter coefficient, W_r is the compressed pulse envelope in the range direction, ω_a is the received signal strength as the function of azimuth time, η_c is the beam center-crossing time, R_0 is the range of the closest approach to a target, and K_a is the azimuth FM rate. This approximation is valid for the low-squint case. The azimuth FM rate in the zero-squint case is derived as follows:

$$K_a = \frac{2}{\lambda}\frac{d^2R(\eta)}{d\eta^2}\bigg|_{\eta=\eta_c} = \frac{2V_{\text{auto}}^2}{\lambda R_0}. \tag{7}$$

The azimuth FM rate involves the azimuth-matched filter, which is applied to focus the data in the azimuth direction after RCMC of RDA. The matched filter for an azimuth compression is expressed as follows:

$$H_a(f_\eta) = \exp\left\{-j\pi\frac{f_\eta^2}{K_a}\right\}. \tag{8}$$

Equation (8) is a complex conjugate of the last exponential term in (6) after azimuth fast Fourier transform (FFT) of RDA. The velocity of the automobile platform is significantly lower than the velocity of satellites and airplanes; this means that the azimuth FM rate of the automobile SAR is less than the rate of the airborne and spaceborne SARs from (7). Therefore, in the automobile SAR, the bandwidth of the matched filter is extremely narrow when the PRF is high enough to avoid the azimuth ambiguity in accordance with (8). For the proof of the above fact, we carry out a matched filter simulation in cases of an automobile, an airplane, and a satellite with the following parameters: carrier frequency 14.25 GHz, PRF = 5000 Hz, FFT size = 8192 bins, the target exposure time 1 s, the automobile velocity 22.22 m/s, the airplane velocity 88.89 m/s, the satellite velocity 3000 m/s, the range of the closest approach with the automobile 400 m, the range of the closest approach with the airplane 4 km, and the range of the closest approach with the satellite 840 km. The results are shown in Fig. 2. Fig. 2 shows that the matched filter in the automobile SAR signal processing operates like a low pass filter with the less narrow bandwidth compared to the other radar platforms. For this reason, in the range-Doppler domain of the automobile SAR, a region near to the zero Doppler frequency is dominant in obtaining a clear image under a single-look processing.

III. Proposed Reconstruction Scheme Through Scaled CS

A. CS

To guarantee the complete reconstruction of an original signal, a frequency of twice its bandwidth is configured as the sampling rate in the data acquisition process according to the Shannon–Nyquist sampling theorem. However, CS has been recently introduced as an attractive alternative [20], [21]. This theory can reconstruct sparse or compressible signals with much fewer measurements than the number of samples required by the Nyquist theorem. In this section, we briefly introduce the concept of CS.

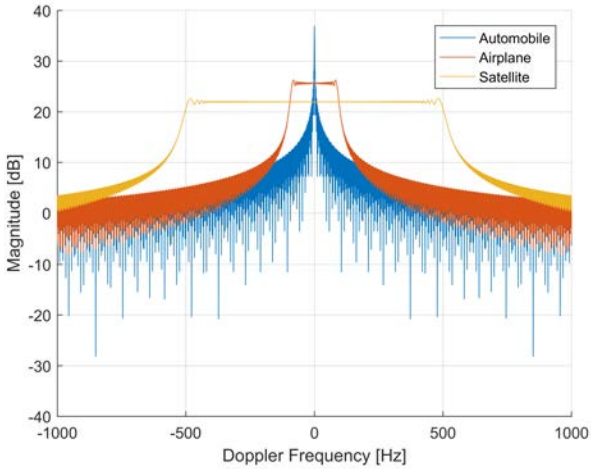

Fig. 2. Matched filter simulation for azimuth compression when radar platforms are an automobile, an airplane, and a satellite.

Let us consider that $y_{\text{total}} \in \mathbb{R}^N$ is L-sparse in a basis, which can be mathematically modeled as follows [13], [22]:

$$y_{\text{total}} = \Psi x \tag{9}$$

where Ψ is an $N \times N$ transformation matrix. In this paper, we utilize the inverse fast Fourier transform (IFFT) as a transformation matrix to recover a scene. x is an $N \times 1$ column vector with L nonzero elements, which means that $\|x\|_0 = L \ll N$. Suppose that the N coefficients of the signal x are not obtainable from direct measurement. We obtain an $M \times 1$ linear measurement vector $y \in \mathbb{R}^L$ using an $M \times N$ measurement matrix Φ from y_{total} with $L < M \ll N$. The measurement matrix means that we measure fewer samples from the vector y_{total}. Equation (9) can be rearranged in terms of the matrices introduced above

$$y = \Phi\, y_{\text{total}} = \Phi\Psi\, x = \Theta\, x \tag{10}$$

where Θ is a sensing matrix. As $M < N$, it is impossible to obtain a unique solution by solving (10). However, the signal x is sparsely representable, which means that the reconstruction of signal x from measurements y is available. The signal x can be recovered exactly by solving the following l_1-minimization problem:

$$\hat{x} = \arg\min \|x\|_1 \text{ such that } y = \Theta\, x. \tag{11}$$

Using linear programming methods, this optimization problem can be solved. For a more realistic case, (10) can be rearranged by adding measurement noise [22]–[24]

$$y = \Theta\, x + \eta \tag{12}$$

with $\|\eta\|_2 \le \varepsilon$, which means that ε is an upper bound of the l_2-norm of noise. In other words, ε is determined by the noise

power. In our case, the noise is assumed to be white Gaussian noise, according to the central limit theorem, because it is caused by an infinite number of sources in a realistic case [25]. Several optimization problems can be used to obtain a signal closest to the original

$$\widehat{x} = \arg\min \|x\|_1 \text{ such that } \|y - \Theta x\| \leq \varepsilon. \tag{13}$$

We exploit this optimization problem, also known as BPDN, to achieve a sparse scene recovery of our automobile FMCW SAR.

B. Feasibility Study on CS FMCW SAR

From Section III-A, the following three conditions can be summarized to apply CS to sparse reconstruction [23].

1) The vector x is sparse and compressible.
2) The number of measurements should satisfy the following inequality:

$$M \geq cL \log \frac{N}{L}. \tag{14}$$

3) The sensing matrix Θ plays a key role in estimating the sparse vector x from the undersampled signal y. The sensing matrix should follow the restricted isometric property (RIP), which is

$$(1 - \delta_L)\|x\|_2^2 \leq \|\Theta x\|_2^2 \leq (1 + \delta_L)\|x\|_2^2 \tag{15}$$

where δ_L is an isometry constant. This is the smallest constant among the constants satisfying (15). An isometry constant close to zero ensures that the sensing matrix has satisfactory RIP; this enables recovery with CS to reconstruct the undersampled signal perfectly with high probability.

In general, as a simple solution, random sampling is selected to bring the isometry constant closer to zero. For this reason, we utilize a random sampling matrix as the measurement matrix for sparse reconstruction. Under these conditions, the signals restored with CS are the same because it guarantees perfect recovery even with different samples. Conversely, if the three mandatory conditions are not met, the results reconstructed with different samples can be different.

Let us examine the applicability of CS to the FMCW SAR dataset from these conditions. The applicability can be seen by considering CS reconstruction along a range or azimuth direction of the dataset because we use IFFT as a transformation matrix of (9). First, we consider the feasibility of CS reconstruction along the range direction in FMCW SAR. We extract range information of a target using FFT, which is a simple process as a range compression stage compared to the conventional pulsed SAR. In other words, after range FFT, each frequency component in the frequency domain denotes the range information of each target. For a typical SAR simulation, a few stationary targets in a scene are assumed as scatterers for easy implementation. After range FFT, only a few beat frequency components in the frequency domain are generated by a few scatterers. Therefore, the signal is sparse and compressible in a frequency basis; this enables undersampled raw data in the range direction to be applied by CS for a sparse reconstruction [13]. However, in a realistic case, there are countless scatterers on the ground, which means that the signal in the frequency domain is not sparse and compressible. For this reason, in the range direction, the CS method is not applicable to exactly reconstruct the subsampled data or data loss of FMCW SAR.

Second, a signal in the azimuth direction is also not sparse and compressible in the frequency domain. Nevertheless, in the case of automobile FMCW SAR, note that the azimuth compression-matched filter has an extremely narrow bandwidth, as mentioned in Section II. Thus, the low-frequency signal within the bandwidth of the filter is essential to produce an automobile SAR image because of the narrow filter. Suppose that the other frequency data are noise because the data are not essential for providing a defined SAR image. We can then assume that the signal within the bandwidth, which should be used in azimuth compression, is sparse and compressible. Through this approach, we identify that a typical CS is applicable to the subsampled signal along the azimuth direction for the sparse recovery. On the other hand, if the three requirements for perfect reconstructions cannot be completely met, the typical CS does not ensure to perfectly reconstruct the low-frequency signal in the Doppler domain. This is because CS mainly focuses on all frequency data recovery under the unsatisfactory conditions. To overcome this, we will introduce scaled CS with its improved recovery performance for low-frequency signals in Section III-C.

C. Scaled CS

As mentioned in Section III-B, low-frequency data in azimuth are significant for producing automobile FMCW SAR images. In this section, we propose a new CS scheme, called scaled CS, to improve the recovery performance for low-frequency data along the azimuth direction for each range bin. Scaled CS is defined as follows:

$$\widehat{x} = \arg\min \|x\|_1 \text{ such that } \left\| \frac{1}{k_{\text{scale}}} y - \Theta \left(\frac{1}{k_{\text{scale}}} x \right) \right\| \leq \varepsilon \tag{16}$$

where k_{scale} is a scale factor such that $k_{\text{scale}} > 1$. Equation (16) is based on BPDN.

In case of the automobile FMCW SAR, a low-frequency signal in azimuth has a dominant power level. The relative motion of the radar platform and the target causes a Doppler shift of the received signal. The average Doppler shift in the azimuth direction is called the Doppler centroid, which is proportional to the platform velocity. The centroid should be estimated from a geometry model and the received signal because it is distinctly noticeable in the azimuth direction. However, in case of automobile FMCW SAR, the Doppler centroid estimation is not essential due to the particular slower velocity than the other platforms; this means that the Doppler shift is close to zero if there is no moving target. In addition, the azimuth bandwidth of the received signal is narrow compared to that of other radar platforms. In a zero-squint mode, azimuth bandwidth of a target can be described as follows [19]:

$$\Delta f_{\text{dop}} = \left| \frac{2V_{\text{auto}} \cos\theta_{r,c}}{\lambda} \theta_{\text{bw}} \right| = \frac{2V_{\text{auto}}}{\lambda} \theta_{\text{bw}} \tag{17}$$

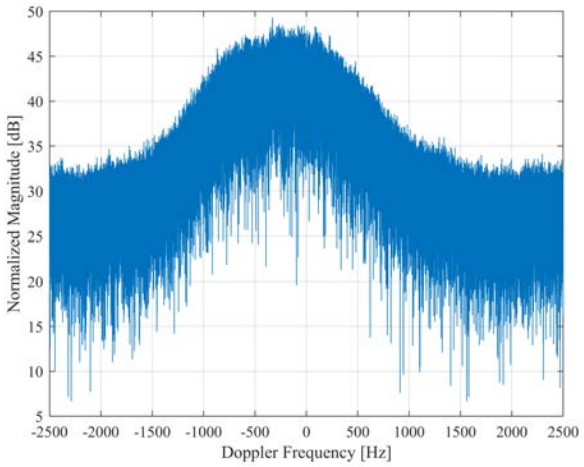

Fig. 3. Azimuth raw signal in the Doppler domain, which is extracted at the same range bin of the real raw data matrix measured in our field test.

where θ_{bw} is the 3-dB width of the radar beam. Equation (17) indicates that the automobile SAR produces a narrower azimuth bandwidth of the received signal as compared to other SAR platforms. Fig. 3 shows azimuth raw data in the Doppler domain, which are extracted at a range bin of real raw data matrix measured in our field test. We can check that the power level of the low frequency is considerably higher than that of the high frequency. For these reasons, the low-frequency information in azimuth has a dominant impact on providing an automobile SAR image because of both the large magnitude of the low-frequency signal and the extremely narrow azimuth-matched filter. The proposed method, therefore, focuses on the low-frequency signal reconstruction. As the power level of the low frequency is dominant, we can assume the other frequency signal to be noise. By expanding ε in (13), we can consider the high-frequency signal to be noise. Because its magnitude is as small as negligible, this enables sparse reconstruction with CS to concentrate on the low-frequency region within the bandwidth of the azimuth-matched filter. In this regard, the simply modified optimization problem is defined as follows:

$$\widehat{x} = \arg\min \|x\|_1 \text{ such that } \|y - \Theta\ x\| \leq k_{\text{scale}}\varepsilon. \quad (18)$$

However, directly expanding the error range in (18) requires a long computational time. Thus, we propose (16) by transposing the scaled parameter k_{scale} to have the same effect on (16) as that with (18). To compare the performances of (16) and (18), we conduct a signal recovery simulation with azimuth data (500 samples) acquired from our field test. We measure the elapsed time of the signal recovery 1000 times using a different random sampling matrix for each attempt with a stopwatch function. Table I provides the average elapsed time in the simulation to compare the recovery efficiencies of (16) and (18).

Table I shows that the average elapsed time obtained with (16) is shorter than that obtained with (18); this means that our recovery method with (16) is efficient compared to simply expanding the error limit. Thus, we propose the recovery method with (16), scaled CS, as our main concept.

For the proof of the improved performance of our scaled CS, we conduct a simulation in cases of subsampled data

TABLE I
AVERAGE TIME FOR SIGNAL RECOVERY WITH (16) AND (18)

Parameter	Equation (16)	Equation (18)
Average elapsed time [sec]	0.77	1.71

reconstruction in the azimuth direction via a typical CS and a scaled CS. Designing the matrix Θ is an essential problem to achieve an exact reconstruction with CS. Consequently, we use a random slow-time undersampling as the random sampling matrix of Θ to demonstrate the enhanced sparse scene recovery of the scaled CS. This undersampling scheme is defined as sampling at random intervals along the azimuth direction, whereas the basic undersampling is a way to periodically sample data at regular intervals with multiple PRFs. This method enables the sensing matrix Θ to contain satisfactory RIP [26]. Moreover, in terms of hardware, the scheme provides easier implementation than random fast-time undersampling by randomly selecting a few LFM chirps. This sampling plan indicates a minor change in the automobile FMCW SAR system. For these reasons, the reconstruction simulation using randomly undersampled real data (20% of data used) has been performed with the following parameters: total number of data 500 samples, number of subsampled data 100 samples, carrier frequency 14.25 GHz, PRF = 5000 Hz, FFT size = 512 bins, and automobile velocity 22.22 m/s. High PRF enables azimuth data to be more compressible in the Doppler domain; this means that the recovery performance of CS with a high PRF is improved. In this simulation, as PRF is determined by considering various factors, PRF of our SAR system is used for practical cases. We exploit the same random sampling matrix to compare the typical CS and the proposed CS. Fig. 4 shows the reconstructed data in the azimuth direction by using our proposed method (the scale factor is 10) and the original CS. We can check that the signal recovered by our method is sparser and more compressible in the Doppler domain than the signal recovered by a typical CS. The recovered signal with the scaled CS also has a significantly higher magnitude in the low-frequency region. Fig. 4 demonstrates that the scaled CS leads to a better reconstruction of low-frequency data.

Next, we examine another recovery simulation to identify whether the larger scale factor of our method causes a better recovery performance with the mean absolute percentage error (MAPE). In this simulation, we use 16 384 samples as an original signal in the azimuth direction. As the scale value is increased, the randomly undersampled data (10%, 20%, 30%, and 40% of data used) are recovered with our method. In this simulation, the same random sampling matrix is utilized. After the recovery, we compare the original and recovered signal samples (90 samples in our case) within the 3-dB bandwidth of the azimuth-matched filter in terms of magnitude and phase using MAPE. Fig. 5 shows the simulation result of magnitude MAPE versus the scale value of our method. Fig. 6 presents the simulation result of phase MAPE versus scale value of our method. Figs. 5 and 6 indicate that the increasing scale value leads to less-magnitude MAPE and phase MAPE. However, these MAPEs are saturated at a certain number or more.

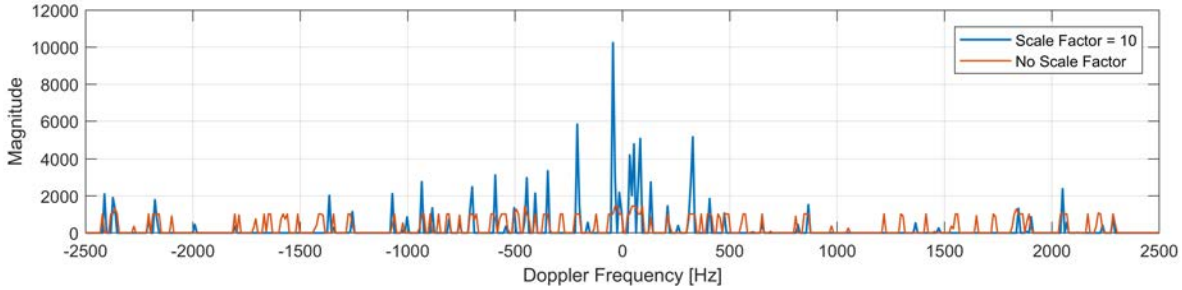

Fig. 4. Simulation result of data reconstruction with scaled CS (scale factor = 10) and the typical CS (BPDN) using randomly undersampled real data (20% of data used). The recovered signal with scaled CS is sparser and more compressible and has a higher magnitude in the low-frequency region than that with typical CS.

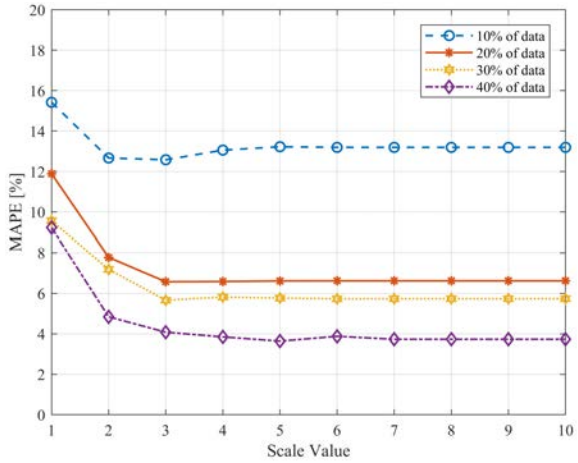

Fig. 5. Simulation result of magnitude MAPE between reconstructed and original signals within the 3-dB bandwidth of the azimuth-matched filter in our case versus the scale value of our method. The 10%, 20%, 30%, and 40% of data are used as subsampled data. Increasing scale value leads to less magnitude MAPE. However, the MAPE is saturated at a certain number or more.

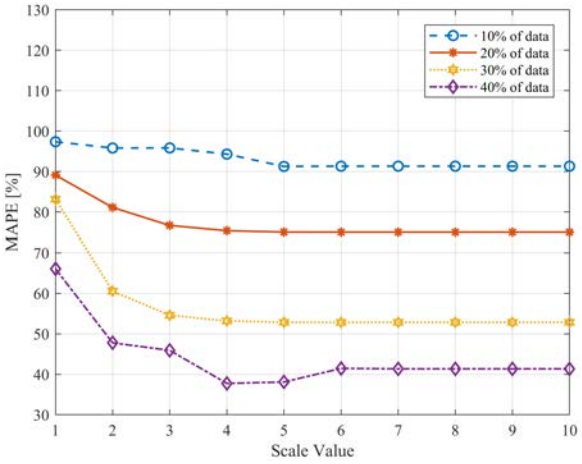

Fig. 6. Simulation result of phase MAPE between reconstructed and original signals within the 3-dB bandwidth of the azimuth-matched filter in our case versus scale value of our method. The 10%, 20%, 30%, and 40% of data are used as subsampled data. Increasing scale value leads to less phase MAPE. However, the MAPE is saturated at a certain number or more.

From these simulation results, this proposed scheme yields an improved performance in terms of low-frequency signal reconstruction in the Doppler domain compared to the conventional CS.

IV. Ku-Band Automobile FMCW SAR System and Experiment

A. Architecture of Ku-Band Automobile FMCW SAR System

We have designed an automobile FMCW SAR system to demonstrate the proposed CS scheme [27], [28]. The system is composed of a DDS, a block upconverter (BUC), a low-noise amplifier (LNA), and USRP N210, as shown in Fig. 7. We apply a type of heterodyne conversion structure to our system. All oscillators of the proposed system are fully synchronized by a reference clock with low phase noise for coherent operation.

In the FMCW radar system, LFM signal generation is extremely important because a nonlinear transmitted chirp signal degrades the range resolution by inducing a broad spectrum and spurious elements of the beat frequency. In fact, the nonlinear signal leads to target range ambiguity. Hence, we utilize a DDS called AD9914 to accurately generate an LFM chirp signal with high linearity. Moreover, to achieve high-resolution SAR images, a wide sweep bandwidth should be simultaneously considered because the range resolution is inversely proportional to the sweep bandwidth. Consequently, the baseband signal in our system periodically sweeps from 950 to 1450 MHz in a 200-μs period from the tradeoff between its sweep time and sweep bandwidth. The flatness of the sweep signal power is guaranteed within the 3-dB frequency domain. The linear DDS signal is mixed with 13.05-GHz low-phase noise in the Ku-band BUC. After the BUC, the signal from 14 to 14.5 GHz is radiated from the Tx-corrugated horn antenna with a power of about 39 dBm. We use two corrugated horn antennas to take advantages of their wider bandwidth, lower sidelobe, and lower cross-polarization than a standard horn antenna.

In the receiver of the designed system, we apply dual IF stages, which can easily overcome an image frequency problem and improve the system selectivity. The received signal reflected to the target is downconverted into the first IF signal after going through the LNA. As a result, an image frequency component is generated by mixing the RF signal with the local oscillator (LO) signal. From the receiver perspective, the image frequency component results in a critical problem that directly distorts the IF region, whereas the component in the transmitter is an unintended spurious component. Moreover, the image frequency rejection on the first IF stage is effective because the first IF causes a wider gap between the LO signal than

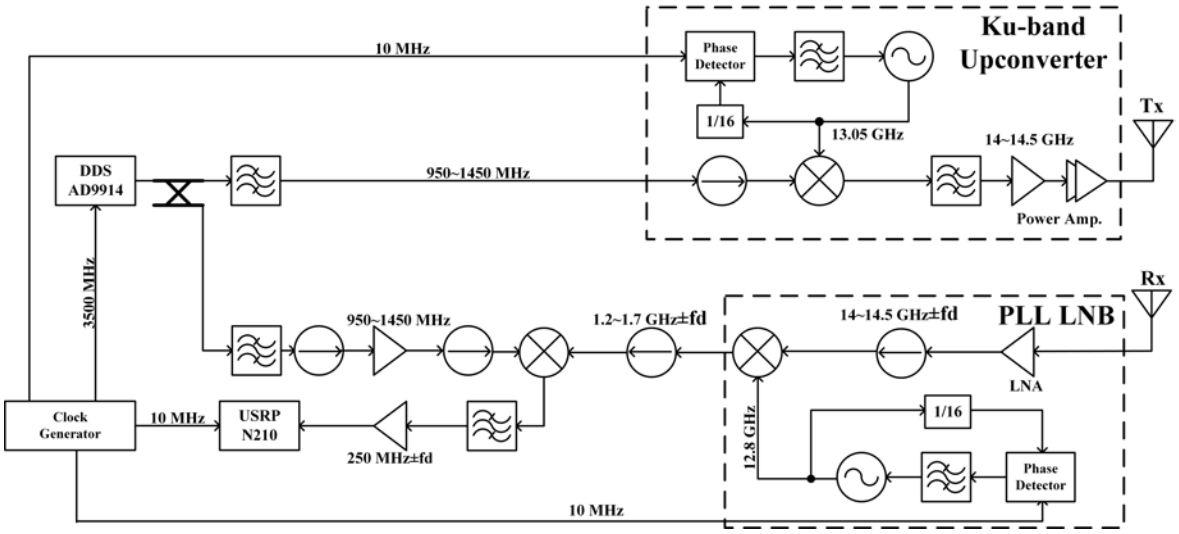

Fig. 7. Block diagram of the Ku-band automobile FMCW SAR system.

TABLE II
SPECIFICATIONS OF THE KU-BAND AUTOMOBILE FMCW SAR SYSTEM

Parameters	Specifications
LFM Sweep Bandwidth	500 MHz
PRI	200 μs
LFM Sweep Type	Sawtooth
Center Frequency	14.25 GHz
Transmission Power	39 dBm
Antenna Type	Corrugated Horn Antenna
Antenna Gain	16 dBi
Antenna 3dB Beamwidth	34°

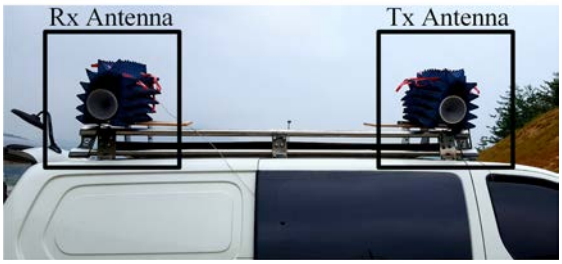

Fig. 8. Tx and Rx antenna configuration on a van.

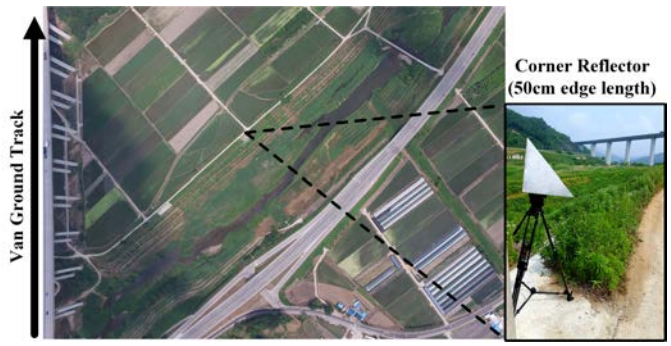

Fig. 9. Aerial photograph of Ku-band automobile FMCW SAR field test site. A trihedral corner reflector was fixed at the center of the test site for the corner reflector profile analysis.

the second one. For these reasons, we insert an isolator at the LNA output to filter out the harmful components. We then add several isolators to prevent a reflected wave. The first IF is

Fig. 10. Ku-band automobile FMCW SAR image field test site. The image covers an area of 555 m (azimuth direction) × 630 m (range direction). This figure shows that our system is valid for automobile FMCW SAR image processing.

mixed down to the second IF to meet the desired selectivity of our system. As the improved selectivity reduces the required Q factor of the RF component, we add a simple low-pass filter through which the second IF is passed into USRP N210.

We then utilize USRP N210 to extract the digital quadrature demodulation data from the filtered signal. In USRP N210, digital signal processing is executed in software based on GNU radio to create a raw data form, producing an FMCW SAR image. Table II provides specifications of the automobile FMCW SAR system.

B. Ku-Band Automobile FMCW SAR Field Test in Stripmap Mode

To evaluate the proposed algorithm, we conduct a Ku-band automobile FMCW SAR field test in the stripmap mode using

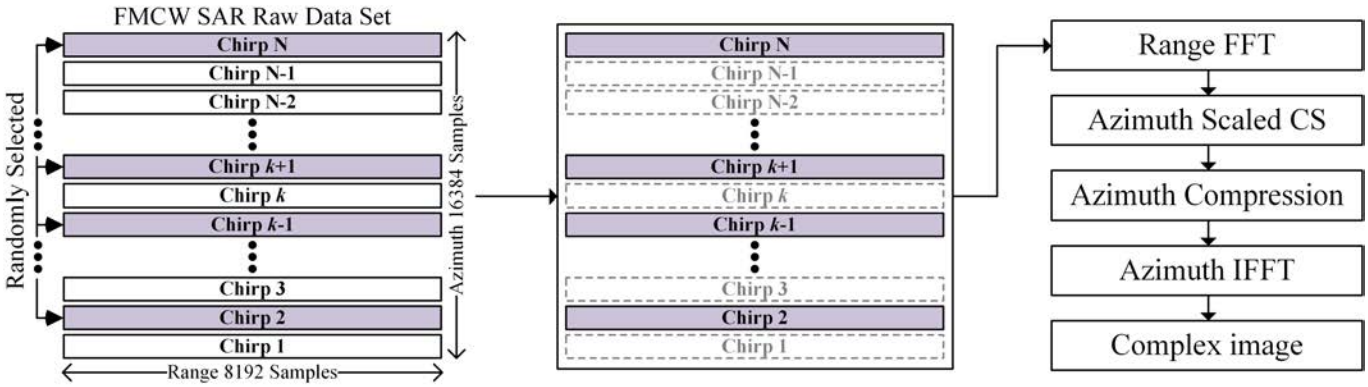

Fig. 11. Proposed sparse scene recovery algorithm for automobile FMCW SAR through scaled CS.

a van on a high bridge, called Saedeul Bridge, in Gong-Ju, South Korea. This bridge rose to a height of about 100 m. The experiment on the high bridge provides a wide observation area, whereas other ground-based SAR experiments provide narrow observation areas. In our case, the observed swath is about 600 m. As shown in Fig. 8, Tx and Rx antennas are mounted on the roof of the van and perfectly aligned toward the ground under the bridge. Except for the mounted components on the roof, the other parts of our system are installed inside the van. We drive the van at a constant velocity of 80 km/h on the bridge, while in-phase and quadrature-phase raw data are automatically saved on a PC. A trihedral corner reflector with 50-cm edge length is fixed on the scene center of the ground for a resolution test, as presented in Fig. 9. After the experiment on the bridge, we process the raw dataset to form an FMCW SAR image by conventional RDA, as shown in Fig. 10. It is obvious that there is no difference between the SAR image and aerial photograph of the test site captured with our drone, as detailed in Fig. 9.This result is clear evidence that the proposed system is valid for automobile FMCW SAR image processing.

V. Real Data Demonstration

A. Proposed Reconstruction Algorithm Through Scaled CS

In this section, to verify the realistic performance of our CS method, we propose a reconstruction algorithm through scaled CS for sparse scene recovery, as described in Fig. 11, which is based on commonly used RDA for SAR image processing. We construct a raw dataset by stacking one chirp corresponding to the received signal during the PRI of our SAR system specifications. As mentioned in Section III-C, we randomly select an arbitrary chirp as the random slow-time undersampling scheme to intentionally construct the missing data set. Then, the dataset is passed on to the range compression stage, where we simply apply the range FFT to the data in the range direction. This is an advantage of FMCW SAR, which can reduce the algorithm complexity and computation time because the range compression in case of pulsed SAR is composed of range FFT, matched filter implementation, and range IFFT.

As the next stage, we add scaled CS to the proposed algorithm, instead of azimuth FFT and RCMC stages, to reconstruct subsampled data in the azimuth direction. We utilize IFFT as the transformation matrix of the scaled CS. Therefore, the recovered data in the frequency domain are obtained after the scaled CS; this means that we can eliminate the need for an additional azimuth FFT.

We remove the RCMC stage because it is not essential for image processing in our case. As a radar platform advances along its path, the distance between the target and the sensor changes. In signal memory, when the variation is larger than the range resolution, this migration through the range cells is called RCM. In general, RCMC is an essential feature for a high-resolution SAR image. However, in our case, the bandwidth of the matched filter for azimuth compression is extremely narrow due to the slow velocity of an automobile, as mentioned in Section II. Therefore, in the range-Doppler domain, the hyperbolic trajectory caused by RCM within the narrow bandwidth is regarded as a straight line. This means that we can produce acceptable enough automobile SAR images without RCMC. A reconstructed image is then finally produced by the proposed reconstruction algorithm after azimuth compression and azimuth IFFT, which are generally used in RDA.

The movement of the sensor within PRI should be considered in case of FMCW SAR because its sweep time is significantly longer than the pulse length of the conventional pulse SAR systems [5], [9], [29], [30]. Nonetheless, the velocity of our automobile platform is sufficiently slow to be supposed stationary during the sweep time compared to aircraft and satellites. For this reason, our algorithm is used for sparse scene recovery under stop-and-go approximation without an additional compensation procedure.

B. Experimental Results and Discussion

To validate our algorithm, we produce an original image (100% data are used) and reconstructed images (20% data are used), as shown in Fig. 12. Fig. 12(a) shows the processed image with typical RDA to evaluate the performance of the reconstruction algorithms with a typical CS and our method. Fig. 12(c) indicates the image recovered with general CS, and Fig. 12(e) illustrates the image reconstructed with scaled CS as our main concept. Fig. 12(b), (d), and (f) shows the cross-range profiles of the trihedral corner reflector visible in the

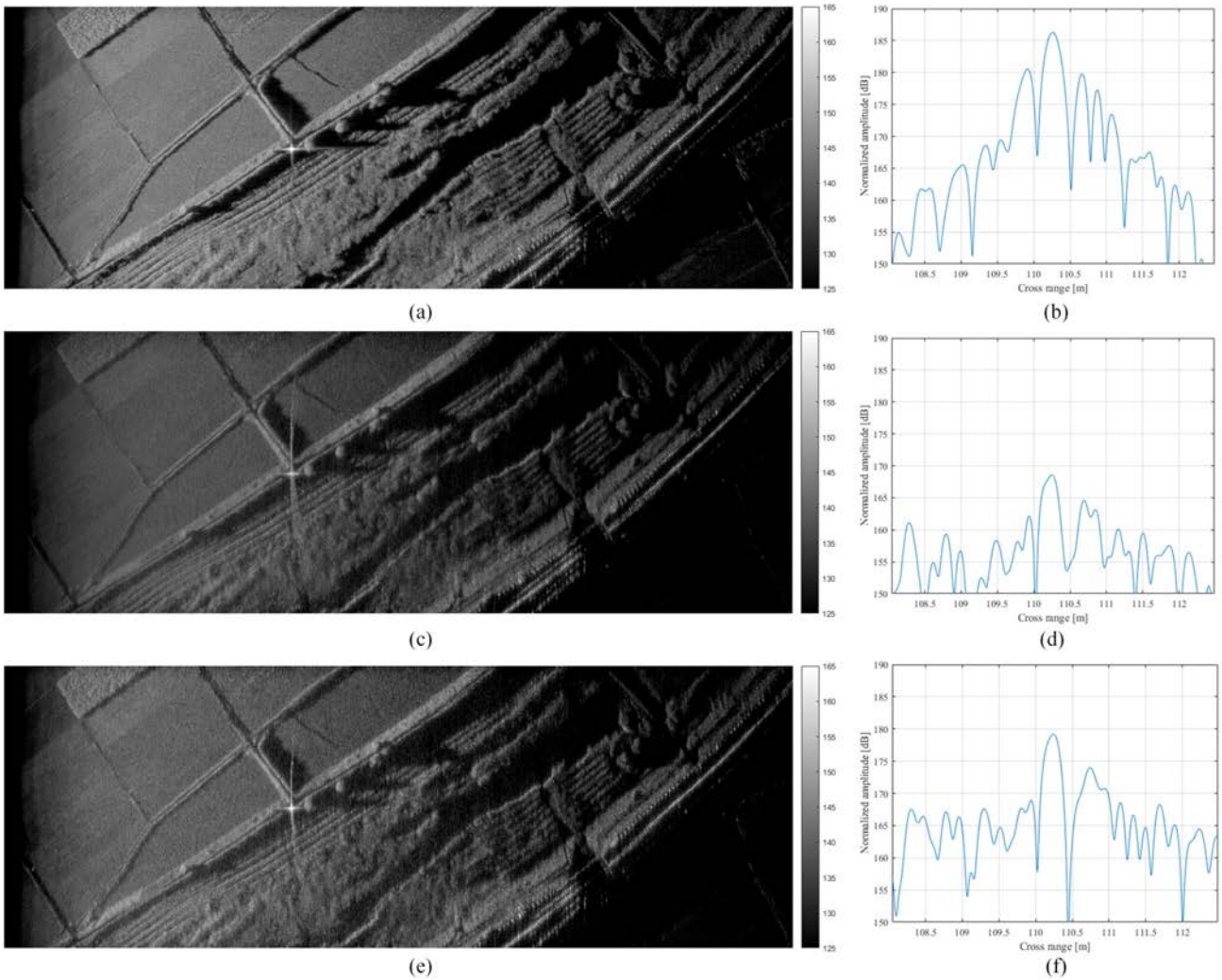

Fig. 12. Experimental results of the processed automobile FMCW SAR images. (a) Original image processed with typical RDA (100% data are used). (b) Cross-range profile of the corner reflector shown in (a). (c) Reconstructed image with typical CS (BPDN) (20% data are used). (d) Cross-range profile of the corner reflector shown in (c). (e) Reconstructed image with the proposed algorithm through scaled CS (20% data are used). (f) Cross-range profile of the corner reflector shown in (e). These SAR images cover an area of 220 m × 630 m. The reconstructed images show considerable reconstruction performance compared to the original image. The reconstructed image with our method indicates that the proposed algorithm through scaled CS has a better ability to recover the subsampled data than the algorithm with a typical CS.

TABLE III

RESULTS OF THE CROSS RANGE PROFILE ANALYSIS WITH THE TRIHEDRAL CORNER REFLECTOR

Parameters	Original image [Fig. 12. (a), (b)]	Reconstructed image with typical CS (BPDN) [Fig. 12. (c), (d)]	Reconstructed image with our method [Fig. 12. (e), (f)]
Peak level [dB]	186.27	168.57	179.18
ISLR [dB]	-6.48	-4.01	-4.56
PSLR [dB]	-5.73	-3.97	-5.21
Azimuth resolution at -3dB [cm]	19.79	21.70	19.88
Azimuth resolution at -10dB [cm]	34.53	33.24	31.64

center of these SAR images detailed in Fig. 12 for cross-range profile analysis.

Compared to the original image, the reconstructed images show considerable scene recovery performance, even though 20% of the original data are used. The image in Fig. 12(c) does not appear to be much different from that in Fig. 12(e) with naked eyes. However, the white vertical solid line of the cross-shape in Fig. 12(e), which indicates the corner reflector, is shorter than the solid line in Fig. 12(c). This shorter solid line indicates better performance for synthesizing cross-range data into a point on the scene. In fact, the proposed reconstruction algorithm with scaled CS has a better ability to recover randomly subsampled data than the algorithm with typical CS in case of automobile FMCW SAR. To evaluate the quality of these recovered images with definite values, we report the results of the cross-range profile analysis with the corner

reflector, as detailed in Table III. We recognize that the peak level increases by almost 10.61 dB. In addition, the integrated sidelobe ratio (ISLR) and the peak sidelobe ratio (PSLR) improve by approximately 0.55 and 1.24 dB, respectively. ISLR is the ratio of the integrated sidelobe power and the integrated main lobe power. PSLR is the ratio of the peak level of the largest sidelobe and that of the main lobe. In our case, we count the area of the single-resolution cell around the maximum peak level as the main lobe. In terms of azimuth resolution at -3 and -10 dB, these reconstructed images are almost the same as the original image. These results indicate that the proposed reconstruction algorithm with scaled CS improves the performance of sparse scene recovery in case of automobile FMCW SAR.

VI. Conclusion

This paper proposed a new method for recovering a sparse scene from the subsampled data of automobile FMCW SAR. Based on the theoretical background presented, the applicability of CS to automobile FMCW SAR was verified. Although it is impossible to perfectly reconstruct the FMCW SAR raw data, we here showed that a sparse scene can be fairly recovered using CS. As described above in detail, low-frequency data in the azimuth direction are important for automobile FMCW SAR, to generate high-resolution SAR images due to an extremely narrow bandwidth of the azimuth-matched filter. Sparse reconstruction using a typical CS is limited because CS is mainly focused on the recovery of all frequency data. Scaled CS was therefore proposed to improve the performance of the low-frequency information recovery from randomly subsampled data. The proposed reconstruction algorithm through scaled CS was validated using the experiment results. The reconstruction performance of the proposed algorithm was described in comparison with a typical CS. Most notably, our method produced a novel approach for restoring a sparse scene with scaled CS, which utilizes the slow speed of the automobile platform.

The combination of FMCW SAR and CS can maximize the benefits, which not only is attractive for conventional aerospace applications but also can meet the commercial needs of new automotive applications. Although FMCW SAR and CS require a long computation time, the related industrial and scientific communities have recently started research to overcome the disadvantage [31]–[34]. Further research should be directed at determining the applicability to millimeter-wave automotive radars with CS and SAR imaging [35]–[37].

References

[1] D.-H. Shin, D.-H. Jung, D.-C. Kim, J.-W. Ham, and S.-O. Park, "A distributed FMCW radar system based on fiber-optic links for small drone detection," *IEEE Trans. Instrum. Meas.*, vol. 66, no. 2, pp. 340–347, Feb. 2017.

[2] G. Hasenaecker, M. van Delden, T. Jaeschke, N. Pohl, K. Aufinger, and T. Musch, "A SiGe fractional-N frequency synthesizer for mm-Wave wideband FMCW radar transceivers," *IEEE Trans. Microw. Theory Techn.*, vol. 64, no. 3, pp. 847–858, Mar. 2016.

[3] S. Scheiblhofer, S. Schuster, and A. Stelzer, "High-speed FMCW radar frequency synthesizer with DDS based linearization," *IEEE Microw. Wireless Compon. Lett.*, vol. 17, no. 5, pp. 397–399, May 2007.

[4] Y. Wang *et al.*, "A 260-mW ku-band FMCW transceiver for synthetic aperture radar sensor with 1.48-GHz bandwidth in 65-nm CMOS technology," *IEEE Trans. Microw. Theory Techn.*, vol. 65, no. 11, pp. 4385–4399, Nov. 2017.

[5] A. Meta, P. Hoogeboom, and L. P. Ligthart, "Signal processing for FMCW SAR," *IEEE Trans. Geosci. Remote Sens.*, vol. 45, no. 11, pp. 3519–3532, Nov. 2007.

[6] Z.-H. Jiang, K. Huang-Fu, and J.-W. Wan, "A chirp transform algorithm for processing squint mode FMCW SAR data," *IEEE Geosci. Remote Sens. Lett*, vol. 4, no. 3, pp. 377–381, Jul. 2007.

[7] W. Q. Wang, Q. Peng, and J. Cai, "Waveform-diversity-based millimeter-wave UAV SAR remote sensing," *IEEE Trans. Geosci. Remote Sens.*, vol. 47, no. 3, pp. 691–700, Mar. 2009.

[8] R. Wang, O. Loffeld, H. Nies, S. Knedlik, M. Hägelen, and H. Essen, "Focus FMCW SAR data using the wavenumber domain algorithm," *IEEE Trans. Geosci. Remote Sens.*, vol. 48, no. 4, pp. 2109–2118, Apr. 2010.

[9] A. Ribalta, "Time-domain reconstruction algorithms for FMCW-SAR," *IEEE Geosci. Remote Sens. Lett.*, vol. 8, no. 3, pp. 396–400, May 2011.

[10] C. He, L. Liu, L. Xu, M. Liu, and M. Liao, "Learning based compressed sensing for SAR image super-resolution," *IEEE J. Sel. Topics Appl. Earth Observ. Remote Sens.*, vol. 5, no. 4, pp. 1272–1281, Aug. 2012.

[11] J. Yang, J. Thompson, X. Huang, T. Jin, and Z. Zhou, "Segmented reconstruction for compressed sensing SAR imaging," *IEEE Trans. Geosci. Remote Sens.*, vol. 51, no. 7, pp. 4214–4225, Jul. 2013.

[12] H. Bu, R. Tao, X. Bai, and J. Zhao, "A novel SAR imaging algorithm based on compressed sensing," *IEEE Geosci. Remote Sens. Lett.*, vol. 12, no. 5, pp. 1003–1007, May 2015.

[13] M. Becquaert, E. Cristofani, and M. Vandewal, "On the applicability of compressive sensing on FMCW synthetic aperture radar data for sparse scene recovery," in *Proc. 10th Eur. Radar Conf.*, Nuremberg, Germany, Oct. 2013, pp. 9–12.

[14] B.-L. Cho, Y.-K. Kong, H.-G. Park, and Y.-S. Kim, "Automobile-based SAR/InSAR system for ground experiments," *IEEE Geosci. Remote Sens. Lett.*, vol. 3, no. 3, pp. 401–405, Jul. 2006.

[15] R. Wang, Y.-H. Luo, Y.-K. Deng, Z.-M. Zhang, and Y. Liu, "Motion compensation for high-resolution automobile FMCW SAR," *IEEE Geosci. Remote Sens. Lett.*, vol. 10, no. 5, pp. 1157–1161, Sep. 2013.

[16] H.-C. Lee, E. S. Kang, S. B. Ryu, S.-G. Lee, S. S. Yong, and C. H. Jung, "Stripmap mode test of X-band AutoSAR prototype using measurement instruments," in *Proc. IEEE IGARSS*, Milan, Italy, Jul. 2015, pp. 1789–1792.

[17] M.-T. Dao, D.-H. Shin, Y.-T. Im, and S.-O. Park, "A two sweeping VCO source for heterodyne FMCW radar," *IEEE Trans. Instrum. Meas.*, vol. 62, no. 1, pp. 230–239, Jan. 2013.

[18] J. Park, S. Park, D.-H. Kim, and S.-O. Park, "Leakage mitigation in heterodyne FMCW radar for small drone detection with stationary point concentration technique," *IEEE Trans. Microw. Theory Techn.*, vol. 67, no. 3, pp. 1221–1232, Mar. 2019.

[19] I. G. Cumming and F. H. Wong, *Digital Processing of Synthetic Aperture Radar Data: Algorithms and Implementation*. Norwood, MA, USA: Artech House, 2005.

[20] D. L. Donoho, "Compressed sensing," *IEEE Trans. Inf. Theory*, vol. 52, no. 4, pp. 1289–1306, Apr. 2006.

[21] E. J. Candès, J. Romberg, and T. Tao, "Robust uncertainty principles: Exact signal reconstruction from highly incomplete frequency information," *IEEE Trans. Inf. Theory*, vol. 52, no. 2, pp. 489–509, Feb. 2006.

[22] V. M. Patel, G. R. Easley, D. M. Healy, Jr., and R. Chellappa, "Compressed synthetic aperture radar," *IEEE J. Sel. Topics Signal Process.*, vol. 4, no. 2, pp. 244–254, Apr. 2010.

[23] A. S. Khwaja and X.-P. Zhang, "Compressed sensing ISAR reconstruction in the presence of rotational acceleration," *IEEE J. Sel. Topics Appl. Earth Observ. Remote Sens.*, vol. 7, no. 7, pp. 2957–2970, Jul. 2014.

[24] F. H. C. Tivive and A. Bouzerdoum, "A compressed sensing method for complex-valued signals with application to through-the-wall radar imaging," in *Proc. IEEE Int. Conf. Acoust., Speech Signal Process. (ICASSP)*, Vancouver, BC, Canada, May 2013, pp. 2144–2148.

[25] M. Jankiraman, *FMCW Radar Design*. Norwood, MA, USA: Artech House, 2018.

[26] R. Baraniuk, M. Davenport, R. DeVore, and M. Wakin, "A simple proof of the restricted isometry property for random matrices," *Construct. Approx.*, vol. 28, no. 3, pp. 253–263, Dec. 2008.

[27] J.-S. Suh, L. Minz, D.-H. Jung, H.-S. Kang, J.-W. Ham, and S.-O. Park, "Drone-based external calibration of a fully synchronized ku-band heterodyne FMCW radar," *IEEE Trans. Instrum. Meas.*, vol. 66, no. 8, pp. 2189–2197, Aug. 2017.
[28] D.-H. Jung and S.-O. Park, "Experimental demonstration of ku-band FMCW automobile-based SAR in stripmap mode," in *Proc. Eur. Conf. Synth. Aperture Radar*, Aachen, Germany, Jun. 2018, pp. 1080–1082.
[29] E. C. Zaugg and D. G. Long, "Theory and application of motion compensation for LFM-CW SAR," *IEEE Trans. Geosci. Remote Sens.*, vol. 46, no. 10, pp. 2990–2998, Oct. 2008.
[30] J. J. M. de Wit, A. Meta, and P. Hoogeboom, "Modified range-Doppler processing for FM-CW synthetic aperture radar," *IEEE Geosci. Remote Sens. Lett.*, vol. 3, no. 1, pp. 83–87, Jan. 2006.
[31] M. Shoaib, K. H. Lee, N. K. Jha, and N. Verma, "A 0.6–107 μW energy-scalable processor for directly analyzing compressively-sensed EEG," *IEEE Trans. Circuits Syst. I, Reg. Papers.*, vol. 61, no. 4, pp. 1105–1118, Apr. 2014.
[32] J.-W. Jhang and Y.-H. Huang, "A high-SNR projection-based atom selection OMP processor for compressive sensing," *IEEE Trans. Very Large Scale Integr. (VLSI) Syst.*, vol. 24, no. 12, pp. 3477–3488, Dec. 2016.
[33] G. Jia, M. Buchroithner, W. Chang, and X. Li, "Simplified real-time imaging flow for high-resolution FMCW SAR," *IEEE Geosci. Remote Sens. Lett.*, vol. 12, no. 5, pp. 973–977, May 2015.
[34] J. Ma, X. Yuan, and L. Ping, "Turbo compressed sensing with partial DFT sensing matrix," *IEEE Signal Process. Lett.*, vol. 22, no. 2, pp. 158–161, Feb. 2015.
[35] H. Yamada, T. Kobayashi, Y. Yamaguchi, and Y. Sugiyama, "High-resolution 2D SAR imaging by the millimeter-wave automobile radar," in *Proc. IEEE CAMA*, Tsukuba, Japan, Dec. 2017, pp. 149–150.
[36] H. Jia *et al.*, "A 77 GHz frequency doubling two-path phased-array FMCW transceiver for automotive radar," *IEEE J. Solid-State Circuits*, vol. 51, no. 10, pp. 2299–2310, Oct. 2016.
[37] J. Vovnoboy, R. Levinger, N. Mazor, and D. Elad, "A dual-loop synthesizer with fast frequency modulation ability for 77/79 GHz FMCW automotive radar applications," *IEEE J. Solid-State Circuits*, vol. 53, no. 5, pp. 1328–1337, May 2018.

Dae-Hwan Jung was born in Seoul, South Korea, in 1988. He received the B.S. degree in electronic and electrical engineering from Sungkyunkwan University, Suwon, South Korea, in 2014, and the M.S. degree in electrical engineering from the Korea Advanced Institute of Science and Technology, Daejeon, South Korea, in 2016, where he is currently pursuing the Ph.D. degree.

His research interests include the design of frequency modulation continuous wave radar systems, frequency-modulated continuous-wave synthetic aperture radar (FMCW SAR), and SAR signal processing.

Hyun-Seong Kang was born in Seoul, South Korea, in 1987. He received the B.S. and M.S. degrees in electrical and electronics from Chung-Ang University, Seoul, in 2012 and 2014, respectively. He is currently pursuing the Ph.D. degree with the School of Electrical Engineering, Korea Advanced Institute of Science and Technology, Daejeon, South Korea.

His research interests include frequency modulation continuous wave radar system, metamaterial, and microwave circuit design.

Chul-Ki Kim was born in Gangneung, South Korea, in 1989. He received the B.S. degree in electronic engineering from Soongsil University, Seoul, South Korea, in 2014, and the M.S. degree in electrical engineering from the Korea Advanced Institute of Science and Technology, Daejeon, South Korea, in 2016, where he is currently pursuing the Ph.D. degree in electrical engineering.

His research interests include synthetic aperture radar (SAR).

Junhyeong Park (GS'18) received the B.S. and M.S. degrees in electrical engineering from the Korea Advanced Institute of Science and Technology (KAIST), Daejeon, South Korea, in 2015 and 2017, respectively, where he is currently pursuing the Ph.D. degree in electrical engineering.

His research interests include frequency-modulated continuous-wave radar system for drone detection, radar target classification, and radar signal processing.

Seong-Ook Park (M'05–SM'11) was born in Yeongcheon, South Korea, in 1964. He received the B.S. degree in electrical engineering from Kyung-Pook National University, Daegu, South Korea, in 1987, the M.S. degree in electrical engineering from the Korea Advanced Institute of Science and Technology (KAIST), Daejeon, South Korea, in 1989, and the Ph.D. degree in electrical engineering from Arizona State University, Tempe, AZ, USA, in 1997.

From 1989 to 1993, he was a Research Engineer with Korea Telecom, Daejeon, where he was involved in microwave systems and networks. He was with the Telecommunication Research Center, Arizona State University, until 1997. Since 1997, he has been a Professor with KAIST. His research interests include antenna, radar system, and analytical and numerical techniques in the area of electromagnetics.

Dr. Park is a member of Pi Kappa Phi.